ACS Catalysis

Research Article

pubs.acs.org/acscatalysis

Active Sites of Au and Ag Nanoparticle Catalysts for CO_2 Electroreduction to CO

Seoin Back,[†] Min Sun Yeom,[§] and Yousung Jung*[,†]

[†]Graduate School of EEWS, Korea Advanced Institute of Science and Technology (KAIST), 291 Daehakro, Daejeon 305-701, Korea

[§]Department of Supercomputing Application, Supercomputing Service Center, Division of National Supercomputing R&D, Korea Institute of Science and Technology Information (KISTI), Daejeon 305-806, Korea

Supporting Information

ABSTRACT: Highly active and selective CO_2 conversion into useful chemicals is desirable to generate valuable products out of greenhouse gases. To date, various metal-based heterogeneous catalysts have shown promising electrochemical catalytic activities for CO_2 reduction, yet there have been no systematic studies of the active sites of these metal catalysts that can guide further experiments. In this study, we use first-principles calculations to identify active sites for the CO_2 reduction reaction for Ag and Au metals, the two metals that have been shown to be the most active in producing CO. We compare the catalytic activity and selectivity of three reaction sites of nanoparticles, namely, low-index surfaces, edge sites, and corner sites of these metals. For nanoparticle corner sites, in particular, we find that the size effect is critical, and 309-atom (or larger) nanoparticles should be used to appropriately describe realistic metal nanocatalysts. However, a 55-atom cluster model is often used in the literature to model nanoparticles. From a comparative study, we reveal that corner sites are the most active for the CO_2 reduction reaction in the case of Au, whereas edge sites are the most active in the case of Ag. Although Au is generally the more active CO_2 reduction catalyst than Ag due to the intrinsically stronger binding of *C-species, our results indicate that reducing the size of Au nanoparticles up to 2 nm also increases the unwanted H_2 evolution reaction, as observed in a recent experiment. However, reducing the size of Ag nanoparticles up to 2 nm enhances the CO_2 reduction reaction without suffering from the H_2 evolution reaction, and on this basis, Ag nanoparticles are a comparable or even better-performing, inexpensive catalyst than Au for electrochemical CO production. Our findings suggest that the catalyst design principle (elemental composition, morphology, and size) is metal-dependent and should be carefully tailored for each system.

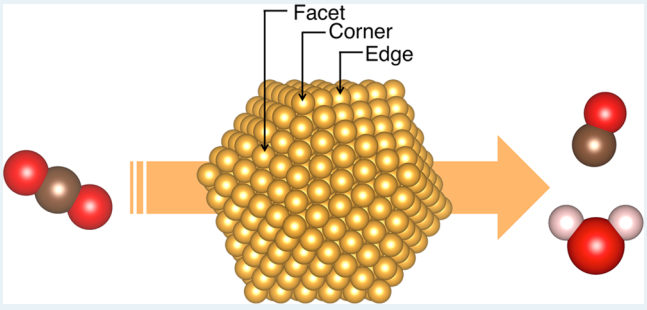

KEYWORDS: *density functional calculations, CO_2 electroreduction, active sites, electrocatalysts, nanoparticles, metal catalysts*

1. INTRODUCTION

Increasing attention has been directed to the CO_2 electroreduction reaction (CRR) as a means to mitigate overproduction of CO_2 and prepare for a fluctuating supply of fossil fuels. Among various methods to convert CO_2, electrochemical reduction is considered a promising way to produce various value-added chemicals from CO_2, partly because the electricity required to drive the reduction reaction can be supplied from sustainable energies, such as wind and solar power.[1,2] The main obstacles for the CO_2 reduction reaction are high electric energy required to obtain reduction products, known as high overpotential, and low selectivity for CO_2 reduction products due to the parasitic H_2 evolution reaction (HER). Theoretically, CO_2 can be converted into various hydrocarbons and alcohols at −0.3 V ∼ +0.3 V (vs a reversible hydrogen electrode (RHE)). However, it was observed that very large overpotential, approximately ∼1 V, should be applied to experimentally reduce CO_2.[3] At the same time, as a sufficiently negative potential is applied, the H_2 evolution reaction becomes problematic. Because unwanted hydrogen gas molecules are produced by consuming protons and electrons, components that are also required in the CO_2 reduction, the HER reduces the faradaic efficiency for CO_2 reduction products. Therefore, to make the CO_2 reduction reaction more active (lower overpotential) and selective (suppressed HER), proper design of new catalysts is a fundamental prerequisite.

Extensive experimental and theoretical studies have been performed to understand the CO_2 reduction reaction.[3−7] After the first comprehensive CO_2 reduction experiments on polycrystalline transition metals,[8] it was suggested from both experiments and theory that the binding energy of CO, a key intermediate of CRR, on the transition metal surfaces determines the overall activity of the CO_2 reduction to produce C1 and C2 hydrocarbons or alcohols.[7] That is, too strongly bound CO may poison the catalyst surface, whereas too weakly

Received: March 4, 2015
Revised: July 5, 2015
Published: July 13, 2015

DOI: 10.1021/acscatal.5b00462
ACS Catal. 2015, 5, 5089−5096

bound CO desorbs off the surface too easily without further protonation. Therefore, optimum CO binding is required, and for that Cu and its derivatives, e.g. oxide-derived Cu[9,10] and Cu nanoparticles,[11] have been investigated to enhance the catalyst performance. On the other hand, when the aim is to produce CO(g) as a simpler CRR product, the focus of the present paper, catalysts should bind *CO weakly enough to remove it from the surface, although they should bind *COOH strongly enough to facilitate the activation of CO_2, where * indicates the surface-adsorbed species. The challenge, however, is that the binding energies of *COOH (E_B[*COOH]) and *CO (E_B[*CO]) are typically proportionally correlated via the so-called scaling relations, making them difficult to control individually.[5]

To develop more active and selective catalysts for CO(g) production from CO_2, several recently suggested approaches have exploited the transition metal nanoparticles (NPs), perhaps motivated by the outstanding catalytic results of NPs for other related reactions, such as CO oxidation,[12,13] the oxygen reduction reaction,[14−17] and the hydrogen evolution reaction.[18,19] The observed enhanced catalytic properties of NPs have been linked to a number of possibilities; an increased catalyst surface per mass and an increase in the number of under-coordinated facets, which bind reaction intermediates more strongly.[20−22] Recent experiments on Ag NPs with various sizes (5−200 nm) revealed that the catalytic activity increased 10-fold as the NP size decreased to 5 nm.[23] In addition to improved current densities by the introduction of NPs, the product selectivity was also substantially affected depending on the different Cu morphologies.[24] More recently, Au NPs have been tested for the CO_2 reduction reaction.[22,25] Using 8 nm Au NPs, the faradaic efficiency (FE) for CO production reached 90% at −0.67 V, indeed an improvement over polycrystalline Au (87% at −0.74 V).[22] Density functional theory (DFT) calculations then suggested that the desired CRR is the most active at the Au edge sites, while the Au corner sites overbind CO, preventing product liberation from the surface. The 8 nm Au NPs are consequently the most selective for the CO product due to having the optimum edge-to-corner ratio. Based on this understanding as a design principle, Au nanowires (NWs) have been investigated since the nanowires have an even higher edge-to-corner ratio than nanoparticles.[26] In comparison to Au NPs, Au NWs indeed showed considerably enhanced CO production selectivity (FE of 94% at −0.35 V). It is, however, unclear whether the same design principle (increased edge-to-corner ratio yielding enhanced CRR activity and selectivity) would hold for other metals. In this regard, systematic studies that clarify the active sites of metal catalysts for CO_2 electroreduction are presently lacking in the literature, despite the large number of experimental and theoretical studies on the CO_2 reduction reaction using metal catalysts. Because many of these former theoretical interpretations of nanoparticles are based on the use of small clusters of metals, consisting of 13 to 55 atoms (far less than the realistic sizes of at least few nm),[22,27,28] it is important to establish the size effect of nanoparticles for the CO_2 reduction reaction for well-studied systems.

In this work, we perform a comparative study on the catalytic properties of low-index planes, edge, and corner sites of Ag and Au face-centered cubic (fcc) metals for the CO_2 reduction reaction to produce CO(g), as well as its competing reactions including the HER and the *OH removal processes. We then link our results with recent experimental observations.

2. MODELS AND METHODS

We performed the density functional calculations (DFT) with the RPBE[29,30] functional and projector augmented wave (PAW) pseudopotential[31] using the Vienna Ab initio Simulation Package (VASP).[32,33] An energy cutoff of 500 eV was used, and atoms were optimized until the residual forces were lower than 0.05 eV/Å. We note in passing that, although the absolute binding energies calculated using RPBE might be uniformly shifted considering the usual performance of RPBE that overestimates the bulk lattice constants of transition metals by around 2%,[30] the relative differences between different faces of the same metal, the present focus, will not be affected.

The (100), (110), and (111) surfaces represent the low-index planes of metal catalysts, while the (211) surface represents the bulk stepped edge site with local under-coordination. We used a (3 × 3) surface unit cell with a four-layer slab for the (100) surface and the (111) close-packed surface, a (2 × 3) surface unit cell with a six-layer slab for the (110) surface, and a (3 × 4) surface unit cell with a four-layer slab for the (211) stepped surface based on the lattice constants of Ag and Au (Ag = 4.09 Å, Au = 4.08 Å), referred to as M(100), M(111), M(110), M(211) (M = Ag, Au) (Figure 1 and Figure S.1). We used (3 × 3 × 1) Monkhorst−Pack mesh of k points for M(100), M(111), and M(110), and (3 × 2 × 1) for M(211). All slabs were spaced more than 20 Å perpendicular to the slab surface to avoid artificial interaction due to periodicity. For slab calculations, adsorbates and the upper two layers were allowed to relax, while the subsurface two layers were fixed to their initial positions.

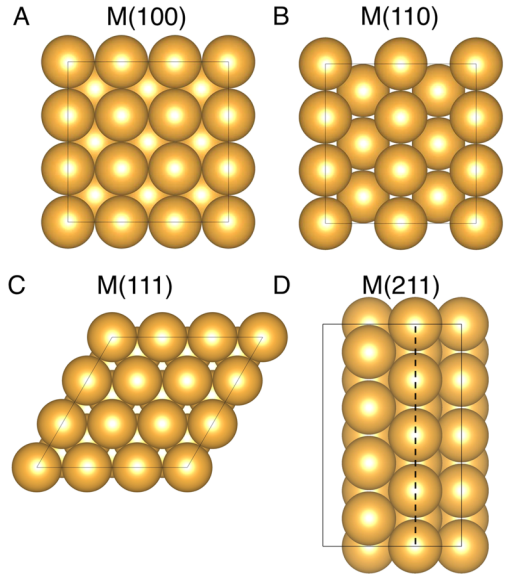

Figure 1. Top views of periodic cells for low-index bulk surfaces, (A) M(100), (B) M(110), (C) M(111), and bulk edge sites (D) M(211). The black lines indicate a unit cell of each surface. The dashed black line in (D) indicates a stepped site.

To model the nanoparticles that properly represent the corner sites of catalysts, we systematically compared *CO and *COOH binding energies of icosahedron nanoparticles at the corner site as a function of particle size (13, 55, 147, 309, 561 atoms) (Figures 2 and 3). Icosahedron nanoparticles with the lattice parameters set to their bulk values (Ag = 4.09 Å, Au = 4.08 Å) and spaced more than 15 Å for all directions were

DOI: 10.1021/acscatal.5b00462
ACS Catal. 2015, 5, 5089−5096

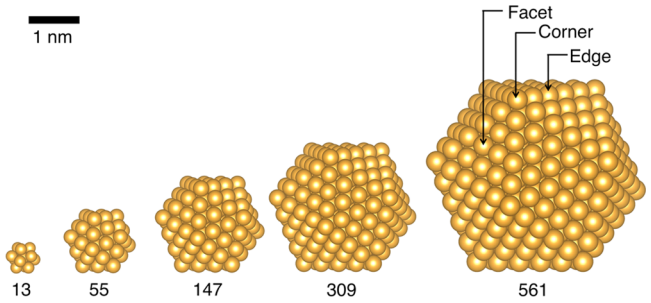

Figure 2. Icosahedron nanoparticles with different sizes used in this study (0.49–2.89 nm).

employed to model the corner sites of metal catalysts. The Brillouin zone was sampled by the gamma point only. During relaxation, nanoparticles were fixed in their initial structures, while adsorbates were relaxed. We note, however, that the binding energy difference of adsorbates between a relaxed and a fixed nanoparticle is negligible for a sufficiently large nanoparticle,[34] which was also confirmed in our study (Figure S.2). In addition to the corner sites, we also considered the edge and facet sites of the nanoparticle using a 309-atom nanoparticle to compare with the bulk (211) and close-packed (111) surface, referred to as M_{309}^{corner}, M_{309}^{edge}, M_{309}^{facet}, respectively. We tested all conventional adsorption sites, namely, atop, bridge, hcp-hollow, and fcc-hollow sites for facet, edge, and corner sites of nanoparticles and used the most stable binding configurations and energies to construct the free-energy diagrams (Figure S.3).

Binding energies of reaction intermediates were calculated as $E_B[*C_xH_yO_z] = E[*C_xH_yO_z] - E[M] - xE[C] - yE[H] - zE[O]$, where $E[*C_xH_yO_z]$ and $E[M]$ denote the calculated electronic energies of M (various surfaces and nanoparticles) with adsorbates and pure M, respectively. $E[C]$, $E[H]$, and $E[O]$ were referenced to the electronic energies of graphene, hydrogen (H_2), and the difference between water and hydrogen ($E[H_2O] - E[H_2]$), respectively. The electronic energy of a stable molecule (CO) was calculated in a large box (10 Å × 10 Å × 10 Å).

To convert electronic energies to experimentally relevant free energies, free-energy corrections and solvation effects should be included. We calculated the zero-point energy, entropy, and heat capacity of adsorbates on Au(111), Au(211), and Au_{13} as well as free molecules, and summed them to yield the free-energy correction. We note that free-energy corrections for Au(111) were used for all low-index facets, while those for Au_{13} were used for Au NPs. See the Supporting Information for all the calculated correction terms (Table S.1, S.2). Because an explicit treatment of the solvation effect is computationally too demanding, we applied an approximate solvation correction scheme for polar adsorbates, as previously calculated on transition metal surfaces. The assumed solvation effects for directly adsorbed *OH and indirectly adsorbed *R−OH through other atoms are −0.5 and −0.25 eV, respectively.[35,36] For *CO, the stabilization was calculated to be −0.1 eV.[5]

To determine free energies of reaction intermediates depending on the external potential, the computational hydrogen electrode (CHE) was employed.[36] CHE assumes that the chemical potential of a proton and electron pair is equivalent to a half of the chemical potential of hydrogen gas at U = 0 V vs the RHE at 101 325 Pa of H_2, 298 K, and all pH values, i.e., $\mu[H^+ + e^-] = 0.5\,\mu[H_2]$. When $U \neq 0$ V vs the RHE, the chemical potential of the proton and the electron pair is shifted by $-eU$, $\mu[H^+ + e^-] = 0.5\,\mu[H_2] - eU$. For every proton−electron transfer step, the potential-dependent chemical potential of a proton−electron pair was used to determine the relative free energy. We note that the proton−electron transfer barrier in each step is assumed to be surmountable at room temperature as the limiting potential is applied.[5]

3. RESULTS AND DISCUSSION

3.1. Nanoparticle Size Dependency of the Corner Site Properties. It is well-known that finite quantum-size effects are introduced when the metal size is decreased to a few

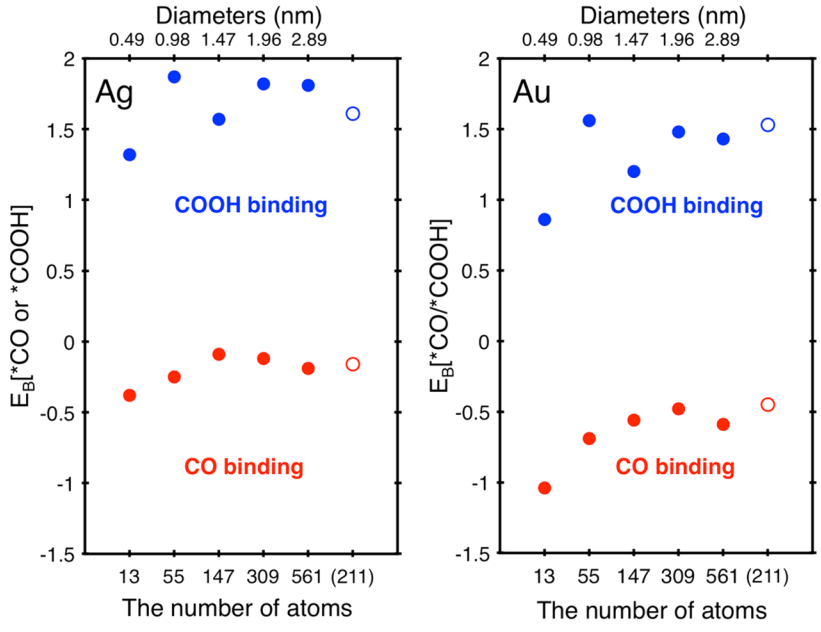

Figure 3. Binding energies (E_B) of *CO (red) and *COOH (blue) at the corner sites of nanoparticles with various sizes. Open circles indicate E_B[*CO] and E_B[*COOH] for the (211) edge sites, respectively.

DOI: 10.1021/acscatal.5b00462
ACS Catal. 2015, 5, 5089−5096

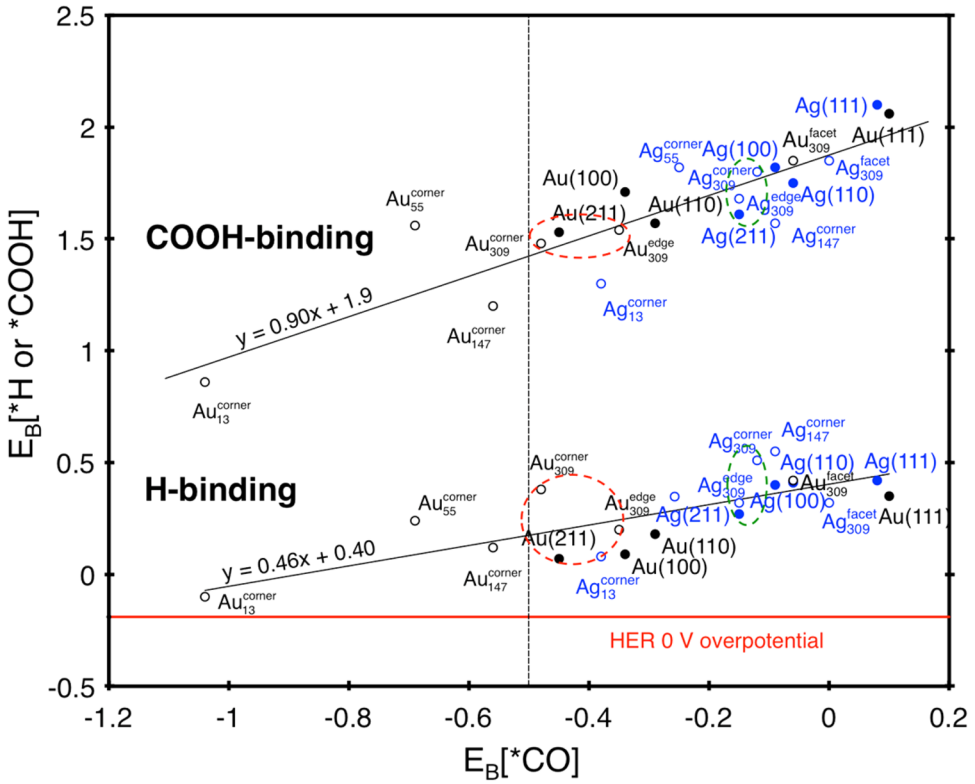

Figure 4. Scaling relation between E_B[*COOH] (upper part) and E_B[*H] (lower part) versus E_B[*CO]. Open circles represent binding energies at nanoparticles, whereas full circles represent binding energies at the bulk surfaces for Ag (Blue) and Au (Black). The vertical dashed line indicates a threshold E_B[*CO] between adsorbed *CO on the catalysts and released CO(g).[5] The horizontal red line indicates E_B[*H] at which the overpotential of HER is 0 V.[42] Dashed green and red circles indicate under-coordinated sites (corner (M_{309}^{corner}) and edge sites (M_{309}^{edge}) of nanoparticles, and the bulk edge site (M(211)) for Ag and Au, respectively. Note that the corner sites of small nanoparticles (M_{13}^{corner}, M_{55}^{corner}, and M_{147}^{corner}) are plotted to build a scaling relation, and only M_{309}^{corner} is discussed in the main text. We note that the binding energy difference between our results and the previous report by Peterson and Nørskov is approximately 0.05 eV, which perhaps arises from different pseudopotentials.[5]

nanometers, which results in intriguing catalytic properties (e.g., inactive bulk Au for CO oxidation becoming active in Au nanoparticles).[37−41] A previous DFT study considered CO and O adsorption on the (211) edge and (111) flat sites of Au nanoparticles with various sizes from 0.8 to 3.7 nm, which correspond to 13-atom and 1415-atom clusters, respectively.[34] It was observed that the quantum-size effects disappear as the size of the nanoparticle increases, that is, a 561-atom (and larger) cluster behaves like the bulk. We note, however, that no systematic studies of the properties of the corner site with varying size have been reported.

We therefore compared the adsorption energies of *COOH and *CO at the corner sites on different sizes of Ag and Au nanoparticle. The results are plotted in Figure 3. Generally, binding strengths become weaker (positive E_B) with increasing size and converge at around 309- or 561-atom clusters. Interestingly, these converged Ag nanoparticles (309 and 561 atoms) at corner sites bind *CO with a strength that is comparable to Ag(211) and bind *COOH more weakly than Ag(211), while Au nanoparticles at corner sites bind *CO and *COOH more strongly than Au(211). Because the difference in binding energies between M_{309}^{corner} and M_{561}^{corner} is less than 0.1 eV, we will discuss the catalytic activity of the corner sites for CO_2 reduction using the M_{309} model. Our calculations indicate that, for converged results, sufficiently large nanoparticle (>309) models must be used to describe realistic nanoparticle catalysts of sizes >2 nm; otherwise, spurious quantum size effects (artificially stronger binding) can appear by using smaller cluster models, which would adversely affect the prediction for NPs larger than 2 nm.

3.2. Comparison of Active Sites for Desired CO_2 Reduction Reaction. The reaction mechanism of CO_2 electroreduction to produce CO(g) is suggested as follows:[4]

$$CO_2 + (H^+ + e^-) \rightarrow *COOH \quad \text{(i)}$$

$$*COOH + (H^+ + e^-) \rightarrow *CO + H_2O(l) \quad \text{(ii)}$$

$$*CO + H_2O(l) \rightarrow CO(g) + H_2O(l) \quad \text{(iii)}$$

The first two steps are potential-dependent electrochemical steps, involving the transfer of a proton−electron pair, while the last step is a thermochemical step that proceeds independently of the biased potential and intrinsically determined by E_B[*CO]. The electrochemical step (i) or (ii) with a higher value of ΔG is the potential-determining step (PDS) and determines the so-called limiting potential ($U_L = -\Delta G_{max}$), defined as the external potential required to make all electrochemical reaction steps thermodynamically downhill. We denote that the first protonation step is the PDS for Ag and Au metal catalysts,[5,43] and thus stabilizing *COOH (more negative E_B[*COOH]) is of great importance to increase the catalytic activity.

The approximate scaling relation between E_B[*COOH] versus E_B[*CO] is illustrated in Figure 4. It is obvious that Au generally binds *C-species (*CO and *COOH) more strongly than Ag, approaching the threshold limit of E_B[*CO] for

DOI: 10.1021/acscatal.5b00462
ACS Catal. 2015, 5, 5089−5096

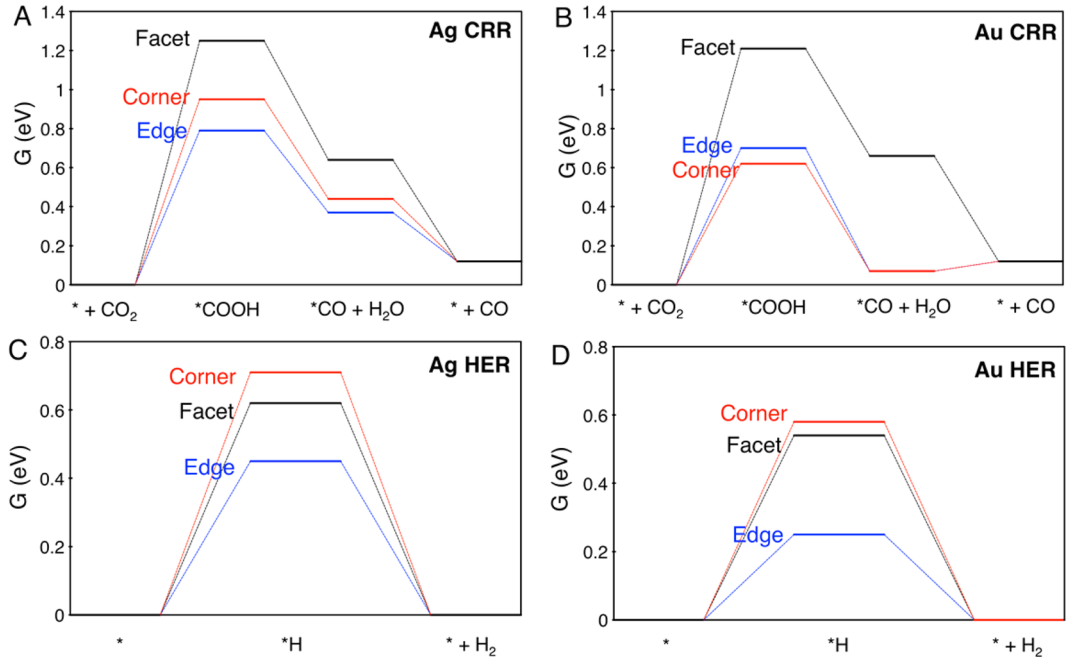

Figure 5. Free energy diagrams for CO_2 reduction reaction (A, B) and H_2 evolution reaction (C, D) on Ag (left) and Au (right). Facet, edge, and corner sites are represented by M(111), M(211), and M_{309}^{corner}, respectively.

under-coordinated sites of Au (Au_{309}^{corner}, Au_{309}^{edge}, and Au(211)). This leads to stabilization of *COOH due to the scaling relation, indicating that smaller overpotential is required for Au than Ag to activate CO_2 to *COOH. Experimentally, polycrystalline Au was observed to yield higher current densities at the same potential for catalyzing CO_2 than polycrystalline Ag.[6] Considering the calculated E_B[*COOH] at low-index surfaces (M(100), M(110), M(111)) of Ag and Au, which are dominant at polycrystalline metal phases, all Au surfaces bind *COOH more strongly than the Ag counterparts. This indicates that Au is more active than Ag for catalyzing CO_2 (Figure 4 and Figure S.4), consistent with polycrystalline experiments. Binding strength is then significantly enhanced as binding sites change from low-index surfaces to under-coordinated sites, although the difference in binding energies among different under-coordinated sites is rather minor. We note that E_B[*COOH] and E_B[*CO] on facet sites of nanoparticles (Ag_{309}^{facet}, Au_{309}^{facet}) are as weak as bulk (111) surfaces, indicating that they are inactive for the CO_2 reduction reaction.

The free-energy diagrams for the CO_2 reduction reaction are summarized in Figure 5A,B. We use free energies of M(111) to represent the facet because M(111) is the most stable low-index facet among the planes. For Ag, G(*COOH) of facet, edge, and corner sites is 1.25, 0.79, and 0.95 eV, respectively, showing that the edge sites are most active for CO_2 reduction. On the other hand, for Au, G(*COOH) of facet, edge, and corner sites is 1.21, 0.70, and 0.62 eV, respectively, suggesting that the corner sites of Au are the most active for CO_2 reduction. We will discuss the overall catalytic performance (activity and selectivity) of active sites for CO_2 reduction in the last section.

3.3. Competing Reactions (HER and *OH Removal). It is essential to consider competing reactions (HER and *OH removal) against CRR to properly evaluate catalysts, because the latter two reactions can significantly impede the catalytic activity for the desired reaction. The HER consists of two consecutive proton−electron pair transfer steps:

$$* + (H^+ + e^-) \rightarrow *H \quad \text{(ia)}$$

$$*H + (H^+ + e^-) \rightarrow * + H_2 \quad \text{(iib)}$$

In order not to be affected by the HER, the limiting potential of the HER should be as negative as possible, with either very weak *H binding or very strong *H binding, as can be found in the volcano plot for the HER.[36,42] Among the latter two possibilities, however, it has been suggested that a weak *H binding is preferred because excessively strong E_B[*H] can block (or poison) the catalytic active sites for CO_2 reduction by preoccupation.[42,44]

In Figure 4, the approximate scaling relation between E_B[*H] versus E_B[*CO] is plotted. The linearly fitted lines for E_B[*COOH] versus E_B[*CO] and for E_B[*H] versus E_B[*CO] demonstrate that the former has a 2-fold larger slope than the latter, which indicates that E_B[*H] is less sensitive to E_B[*CO]. It is clear that E_B[*H] is stronger on Au than Ag, meaning that Au catalysts have smaller overpotential for HER than Ag. In particular, Au(100) and Au(211) bind *H most strongly among the various Au sites, and these sites are expected to produce H_2 readily. In the case of Ag, E_B[*H] is sufficiently weaker than Au, indicating that Ag is less prone to produce H_2. However, rather minor effects can be found in different geometries, less than 0.1−0.2 eV binding energy difference for edge, corner, or facet sites for both Ag and Au, unlike the COOH binding energy, which has a large variation between different geometries (~0.5 eV) within the same metal.

The free-energy diagrams for the H_2 evolution reaction are summarized in Figure 5C,D. Due to the scaling relation, active sites that catalyze CO_2 easily are usually active for catalyzing the HER, demonstrating that Au is more active for the HER than Ag. For both Ag and Au, edge sites can catalyze the H_2 evolution reaction most actively, followed by facet and corner sites. It is noticeable that Au corner sites that are the most

DOI: 10.1021/acscatal.5b00462
ACS Catal. 2015, 5, 5089−5096

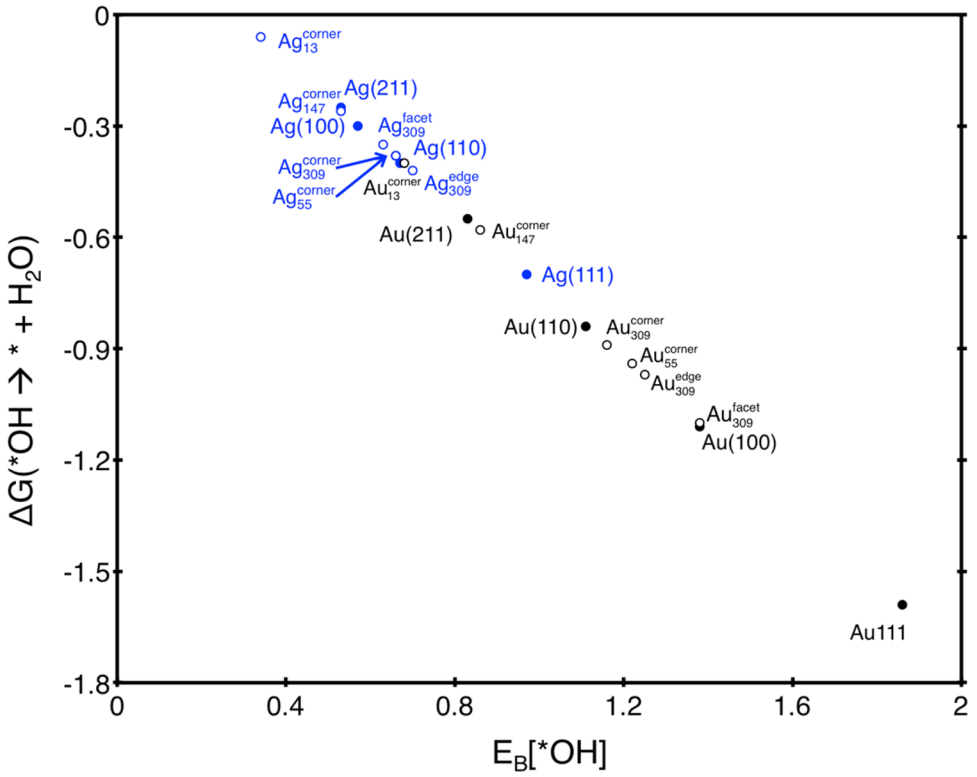

Figure 6. Free-energy changes for *OH removal reaction are plotted versus E_B[*OH]. The same notations are used as in Figure 4. All cases considered here for Ag and Au indicate a thermodynamic downhill for the *OH removal process.

active for the CO_2 reduction reaction are the least active for the H_2 evolution reaction.

The occupation of catalytic active sites not only by *H but also by *OH is problematic because it requires external energies to clear active sites. It was observed experimentally that −0.4 V is required to produce H_2 during the CO_2 reduction reaction on Cu[3], although the calculated limiting potential for the HER was only −0.03 V.[4] This phenomenon was explained with the *OH removal process; a potential of −0.3 V (the theoretical limiting potential) should be applied to clear adsorbed *OH from the Cu (211) stepped site.[4] Therefore, the free-energy change (ΔG) of the *OH removal reaction ($*OH + (H^+ + e^-) \rightarrow * + H_2O$) should be thermodynamically downhill or at least smaller than that of CRR so that *OH is converted to water before CRR begins. As can be seen in Figure 6, we expect that the active site occupation by *OH on those catalysts would not affect the desired CRR because the free-energy changes for the *OH removal process for all sites are negative (favorable). Notably, whereas the *CO affinity is higher for Au than Ag, the *OH affinity is lower for Au than Ag, which indicates a highly resistant nature of Au oxidation.

3.4. Overall Catalytic Performance of Active Sites for CO_2 Reduction Reaction. By combining the results of CRR and HER activity, we can understand the overall performance for the CO_2 reduction reaction at various metal sites for Au and Ag (Table 1). Well-summarized experimental results of Au- and Ag-based catalysts showed that −0.9 V and −1.2 V of overpotential is required to reach 80% of the CO faradaic efficiency for polycrystalline Au and Ag, respectively.[45] Assuming that the low-index surfaces account for most of the polycrystalline phases, our results indicate that Au(100) and Au(110) are more active for CRR than Ag(100) and Ag(110)

Table 1. Summary of G(*COOH) and G(*H) for CRR and HER on Various Sites

(eV)	Ag			Au		
	facet	edge	corner	facet	edge	corner
G(*COOH)	1.25	0.79	0.95	1.21	0.70	0.62
G(*H)	0.62	0.45	0.71	0.54	0.21	0.58

Facet, edge, and corner sites are represented by M(111), M(211) and M_{309}^{corner}, respectively.

due to 0.18 and 0.11 V lower calculated overpotential for Au, consistent with the aforementioned experiments (Figure S.4). In the experiments, the selectivity for H_2 was ∼10% for both metals, which can also be attributed to relatively high calculated overpotentials for the HER on these facet sites (Figure 5).

For nanoparticles, on the other hand, experimentally Ag NPs (5 nm) yielded 1.2 mA/cm^2 of current density at −0.75 V,[23] while Au NPs (4.3 ± 1.3 nm) yielded 5.0 mA/cm^2 of current density at −1.2 V.[28] It is noticeable that 1.0 out of 1.2 mA/cm^2 is responsible for CO production on Ag NP, while the most current density on Au NPs was due to H_2 production.[28] Our results for low-coordinated facets indicate that the Au edge sites more easily produce H_2 than Ag with a low overpotential of −0.21 V for the HER, while the Ag edge sites are slightly less active than the Au corner sites for the CO_2 reduction reaction (G(*COOH): 0.79 eV vs 0.62 eV). Considering both current density and CO selectivity over the HER, our results suggest that the catalytic performance of CO_2 reduction for Ag NPs is quite comparable to, or even better than Au NPs, although there are not yet direct comparative experimental measurements for CO production current density for Ag and Au NPs under the same conditions.

DOI: 10.1021/acscatal.5b00462
ACS Catal. 2015, 5, 5089−5096

3.5. Link to the Experimental Observations. It is helpful to connect the theoretical results to experimental observations.

(i) A previous work by Hori considered facet effects, where current densities for CO_2 reduction on the Ag(110) facet are higher by a factor of 2 than on the Ag(111) or Ag (100) surfaces.[46] The present calculations indicate that the Ag(110) surface binds *COOH most strongly among the other facets (Figure S.4). Therefore, the effect of different facets on the CRR catalytic activity is explained by the calculated binding strength of *COOH.

(ii) Salehi-Khojin and Masel observed increasing current densities for the CO_2 reduction reaction when the size of Ag NPs decreases from 200 to 5 nm, while 1 nm NPs yielded significantly decreased current density.[23] On sufficiently large NPs in a size range of 5−200 nm, quantum-size effects do not exist, and thus, edge sites are the most active sites, as found in this study. We ascribe the improved CO_2 reduction activity on 5 nm Ag NPs mainly to the increased ratio of edge sites, while smaller sized Ag NPs have many corner sites that are much less active.

(iii) A previous DFT study on Au corner (using Au_{13} cluster model) and Au edge sites (using Au(211) stepped surface) suggested that Au edge sites are the key active sites for efficient CO_2 reduction and limited hydrogen evolution reactions,[22] and this was experimentally supported by the observation that longer Au nanowires (NWs) perform better than shorter Au NWs.[26] The present calculations using larger NPs of more realistic size (Au_{309}) suggest that the corner sites of Au rather than the edge sites are the most active CRR and least active HER sites for Au. The experimentally observed higher activity of Au NWs compared to Au NPs might then be due to the possibility that, in addition to the edge sites being the most abundant active (albeit less selective) sites in NWs, the catalytic activities and selectivity of edge sites in NPs and NWs (or the corner sites of the two morphologies) could be quite different toward CRR and the HER due to different local environments in NPs and NWs.

4. CONCLUSIONS

We systematically studied the active sites of Ag and Au nanoparticle catalysts for the electrochemical CO_2 reduction reaction. The main findings of this work are as follows.

(i) The systematic comparison of the corner sites of NPs with different sizes suggests that quantum-size effects are significant at small size NPs. Therefore, sufficiently large NPs (309-atom or more) should be employed to theoretically analyze the catalytic properties of experimental NPs of sizes >2 nm. Model studies using smaller nanoparticles can yield results that are not converged and artificial.

(ii) For Ag and Au that bind reaction intermediates weakly at their low-index facets, the under-coordinated sites are the main active sites for the CO_2 reduction reaction. In particular, for Au, the corner sites are the main active sites, whereas for Ag, the edge sites are the most active. For the H_2 evolution reaction, the edge sites are the most active for both Au and Ag, followed by the facet and corner sites.

(iii) A general trend of strong binding for *C-species on Au explains why polycrystalline Au is more active than polycrystalline Ag. However, Au is also more prone to produce H_2 gas due to the scaling relation, especially at edge sites. The low CO selectivity experimentally observed at smaller Au NPs can be linked to the large number of edge sites compared to polycrystalline phases in NPs. On the other hand, Ag NPs become more active compared to the polycrystalline phase for CRR due to an increase in the number of highly active edge sites, while they do not suffer from the HER due to high overpotential.

(iv) Considering the CRR activity and CO selectivity over H_2 as well as their nanoparticle size dependence, Ag nanoparticles are an efficient and inexpensive alternative to Au catalysts for electrochemical CO production from CO_2. Our results confirm that the catalyst design principle (elemental composition, morphology, and size) is different and should be adjusted to each candidate metal, and we also illustrate how first-principles calculations can lend an insight into the activities and selectivity of metal catalysts.

■ ASSOCIATED CONTENT

Supporting Information

The Supporting Information is available free of charge on the ACS Publications website at DOI: 10.1021/acscatal.5b00462.

Free-energy correction terms for each structure are summarized. Side views of unit cells are presented. Most stable adsorption configurations of *CO, *COOH, and *H are also summarized. Free-energy diagrams are shown to compare the catalytic activity of low-index planes (PDF)

■ AUTHOR INFORMATION

Corresponding Author

*E-mail: ysjn@kaist.ac.kr.

Notes

The authors declare no competing financial interest.

■ ACKNOWLEDGMENTS

S.B. acknowledges Global PhD Fellowship Program through NRF funded by the Ministry of Education (NRF-2014H1A2A1016055). This research was supported by Agency for Defense Development (UD140047GD), and patrly by a collaborative project (Supercomputing infrastructure service and application) with KISTI funded by Ministery of Science, ICT and Future Planning.

■ REFERENCES

(1) Mikkelsen, M.; Jørgensen, M.; Krebs, F. C. *Energy Environ. Sci.* **2010**, *3*, 43−81.

(2) Gattrell, M.; Gupta, N.; Co, A. *Energy Convers. Manage.* **2007**, *48*, 1255−1265.

(3) Hori, Y. *Electrochemical CO_2 reduction on metal electrodes*; Springer: New York, 2008; Vol. *42*, pp 89−189.

(4) Peterson, A. A.; Abild-Pedersen, F.; Studt, F.; Rossmeisl, J.; Nørskov, J. K. *Energy Environ. Sci.* **2010**, *3*, 1311−1315.

(5) Peterson, A. A.; Nørskov, J. K. *J. Phys. Chem. Lett.* **2012**, *3*, 251−258.

(6) Kuhl, K. P.; Hatsukade, T.; Cave, E. R.; Abram, D. N.; Kibsgaard, J.; Jaramillo, T. F. *J. Am. Chem. Soc.* **2014**, *136*, 14107−14113.

DOI: 10.1021/acscatal.5b00462
ACS Catal. 2015, 5, 5089−5096

(7) Gattrell, M.; Gupta, N.; Co, A. *J. Electroanal. Chem.* **2006**, *594*, 1−19.
(8) Hori, Y.; Kikuchi, K.; Suzuki, S. *Chem. Lett.* **1985**, *14*, 1695−1698.
(9) Li, C. W.; Kanan, M. W. *J. Am. Chem. Soc.* **2012**, *134*, 7231−7234.
(10) Rasul, S.; Anjum, D. H.; Jedidi, A.; Minenkov, Y.; Cavallo, L.; Takanabe, K. *Angew. Chem.* **2015**, *127*, 2174−2178.
(11) Reske, R.; Mistry, H.; Behafarid, F.; Roldan Cuenya, B.; Strasser, P. *J. Am. Chem. Soc.* **2014**, *136*, 6978−6986.
(12) Lopez, N.; Nørskov, J. K. *J. Am. Chem. Soc.* **2002**, *124*, 11262−11263.
(13) Lopez, N.; Janssens, T.; Clausen, B.; Xu, Y.; Mavrikakis, M.; Bligaard, T.; Nørskov, J. K. *J. Catal.* **2004**, *223*, 232−235.
(14) Liang, Y.; Li, Y.; Wang, H.; Zhou, J.; Wang, J.; Regier, T.; Dai, H. *Nat. Mater.* **2011**, *10*, 780−786.
(15) Yang, H.; Vogel, W.; Lamy, C.; Alonso-Vante, N. *J. Phys. Chem. B* **2004**, *108*, 11024−11034.
(16) Chen, S.; Ferreira, P. J.; Sheng, W.; Yabuuchi, N.; Allard, L. F.; Shao-Horn, Y. *J. Am. Chem. Soc.* **2008**, *130*, 13818−13819.
(17) Mazumder, V.; Chi, M.; More, K. L.; Sun, S. *J. Am. Chem. Soc.* **2010**, *132*, 7848−7849.
(18) Li, Y.; Wang, H.; Xie, L.; Liang, Y.; Hong, G.; Dai, H. *J. Am. Chem. Soc.* **2011**, *133*, 7296−7299.
(19) Popczun, E. J.; McKone, J. R.; Read, C. G.; Biacchi, A. J.; Wiltrout, A. M.; Lewis, N. S.; Schaak, R. E. *J. Am. Chem. Soc.* **2013**, *135*, 9267−9270.
(20) Remediakis, I. N.; Lopez, N.; Nørskov, J. K. *Appl. Catal., A* **2005**, *291*, 13−20.
(21) Han, B.; Miranda, C.; Ceder, G. *Phys. Rev. B: Condens. Matter Mater. Phys.* **2008**, *77*, 075410.
(22) Zhu, W.; Michalsky, R.; Metin, O.; Lv, H.; Guo, S.; Wright, C. J.; Sun, X.; Peterson, A. A.; Sun, S. *J. Am. Chem. Soc.* **2013**, *135*, 16833−16836.
(23) Salehi-Khojin, A.; Jhong, H.-R. M.; Rosen, B. A.; Zhu, W.; Ma, S.; Kenis, P. J.; Masel, R. I. *J. Phys. Chem. C* **2013**, *117*, 1627−1632.
(24) Tang, W.; Peterson, A. A.; Varela, A. S.; Jovanov, Z. P.; Bech, L.; Durand, W. J.; Dahl, S.; Nørskov, J. K.; Chorkendorff, I. *Phys. Chem. Chem. Phys.* **2012**, *14*, 76−81.
(25) Mistry, H.; Reske, R.; Zeng, Z.; Zhao, Z.-J.; Greeley, J.; Strasser, P.; Roldan Cuenya, B. *J. Am. Chem. Soc.* **2014**, *136*, 16473−16476.
(26) Zhu, W.; Zhang, Y.-J.; Zhang, H.; Lv, H.; Li, Q.; Michalsky, R.; Peterson, A. A.; Sun, S. *J. Am. Chem. Soc.* **2014**, *136*, 16132−16135.
(27) Gao, D.; Zhou, H.; Wang, J.; Miao, S.; Yang, F.; Wang, G.; Wang, J.; Bao, X. *J. Am. Chem. Soc.* **2015**, *137*, 4288−4291.
(28) Mistry, H.; Reske, R.; Zeng, Z.; Zhao, Z.-J.; Greeley, J.; Strasser, P.; Cuenya, B. R. *J. Am. Chem. Soc.* **2014**, *136*, 16473−16476.
(29) Perdew, J. P.; Burke, K.; Ernzerhof, M. *Phys. Rev. Lett.* **1996**, *77*, 3865.
(30) Hammer, B.; Hansen, L. B.; Nørskov, J. K. *Phys. Rev. B: Condens. Matter Mater. Phys.* **1999**, *59*, 7413.
(31) Blöchl, P. E. *Phys. Rev. B: Condens. Matter Mater. Phys.* **1994**, *50*, 17953.
(32) Kresse, G.; Joubert, D. *Phys. Rev. B: Condens. Matter Mater. Phys.* **1999**, *59*, 1758.
(33) Kresse, G.; Furthmüller, J. *Comput. Mater. Sci.* **1996**, *6*, 15−50.
(34) Kleis, J.; Greeley, J.; Romero, N.; Morozov, V.; Falsig, H.; Larsen, A. H.; Lu, J.; Mortensen, J. J.; Dułak, M.; Thygesen, K. S.; Nørskov, J. K.; Jacobsen, K. W. *Catal. Lett.* **2011**, *141*, 1067−1071.
(35) Tripković, V.; Skúlason, E.; Siahrostami, S.; Nørskov, J. K.; Rossmeisl, J. *Electrochim. Acta* **2010**, *55*, 7975−7981.
(36) Nørskov, J. K.; Rossmeisl, J.; Logadottir, A.; Lindqvist, L.; Kitchin, J. R.; Bligaard, T.; Jonsson, H. *J. Phys. Chem. B* **2004**, *108*, 17886−17892.
(37) Janssens, T. V.; Clausen, B. S.; Hvolbæk, B.; Falsig, H.; Christensen, C. H.; Bligaard, T.; Nørskov, J. K. *Top. Catal.* **2007**, *44*, 15−26.
(38) Hvolbæk, B.; Janssens, T. V.; Clausen, B. S.; Falsig, H.; Christensen, C. H.; Nørskov, J. K. *Nano Today* **2007**, *2*, 14−18.
(39) Daniel, M.-C.; Astruc, D. *Chem. Rev.* **2004**, *104*, 293−346.
(40) Xie, Y.-P.; Gong, X.-G. *J. Chem. Phys.* **2010**, *132*, 244302.
(41) Tang, D.; Hu, C. *J. Phys. Chem. Lett.* **2011**, *2*, 2972−2977.
(42) Back, S.; Kim, H.; Jung, Y. *ACS Catal.* **2015**, *5*, 965−971.
(43) Shi, C.; Hansen, H. A.; Lausche, A. C.; Nørskov, J. K. *Phys. Chem. Chem. Phys.* **2014**, *16*, 4720−4727.
(44) Karamad, M.; Tripkovic, V.; Rossmeisl, J. *ACS Catal.* **2014**, *4*, 2268−2273.
(45) Wu, J.; Yadav, R. M.; Liu, M.; Sharma, P. P.; Tiwary, C. S.; Ma, L.; Zou, X.; Zhou, X.-D.; Yakobson, B. I.; Lou, J.; Ajayan, P. M. *ACS Nano* **2015**, *9*, 5364−5371.
(46) Hoshi, N.; Kato, M.; Hori, Y. *J. Electroanal. Chem.* **1997**, *440*, 283−286.

DOI: 10.1021/acscatal.5b00462
ACS Catal. 2015, 5, 5089−5096